Design and Control of a Novel Unmanned Ground Vehicle

M. Osinuga and A. Lanzon
Control Systems Centre, School of Electrical and Electronic Engineering, The University of Manchester, Sackville Street, Manchester, M13 9PL, U.K.
{*mobolaji.osinuga-2, alexander.lanzon*}*@manchester.ac.uk*

Keywords: Unmanned Ground Vehicle, Unmanned Aerial Vehicle, Modelling, Inverted Pendulum, Robust Control.

Abstract: This paper presents a novel design of a full six-degree-of-freedom, tri-rotor-actuated single-wheeled vehicle. When stationary on the ground, the model of the vehicle mimics an inverted pendulum system, a typical representative of highly nonlinear systems with non-minimum phase and unstable characteristics. The full nonlinear model of the vehicle is derived using Newton-Euler approach, but the objective herein is to balance the single-wheeled vehicle in its unstable upright position as this is a precursor to rolling motion. Robust feedback and Jacobi linearization techniques are invoked on the nonlinear dynamics of the vehicle in the relevant axis for subsequent controller synthesis. The synthesized controllers are verified and compared by means of numerical simulations, where it is shown that the design objective of stabilizing the vehicle in its unstable equilibrium (upright) position is robustly achieved.

1 INTRODUCTION

Unmanned vehicles are usually designed to operate with great agility and rapid maneuver, having applications in both military and civilian spheres, for example, reconnaissance, surveillance, search and rescue, disaster remediation, data and image acquisition of targets, etc. (Kim and Shim, 2003; Valavanis, 2007; Das et al., 2009; Lum and Waggoner, 2011). As a result of rapidly increasing interest in autonomous vehicles, industries and researchers, are encouraged to research new vehicle platforms that aim at more efficient configurations in terms of size, range, autonomy and payload capacity amongst other factors. One of such efficient designs is the tri-rotor Unmanned Aerial Vehicle (UAV) (Salazar-Cruz et al., 2006; Escareño et al., 2008; Prior et al., 2009), which has three axes of rotation from a triangular-shaped orientation of actuation as shown in Figure 1.

This platform has been used in many applications (see (Yoo et al., 2010) and the references therein). Unlike earlier work, it is recognized by the authors that if each of the three rotors is attached to a servo motor that allows change in the axis of rotation of the propeller, then the UAV becomes a full six-degrees-of-freedom (6-DOF) vehicle, capable of fully decoupled thrust and torque vectoring in all the 3D-space. Consequently, the UAV has no nominal upright position. This concept is captured in patent (Crowther et al., 2010) and article (Crowther et al., 2011).

Interestingly, a fascinating and attractive scope to unmanned vehicles is their capability to combine different vehicle types that can operate in multiple environments, for example, air and ground, ground and water, etc. These types of vehicles are able to provide up-close visual surveillance capabilities and manipulations that are unattainable with any single vehicle, as they combine the benefits of different types of vehicles into a collective system by exploiting different vehicle types (Omelchenko, 2004). For instance, an unmanned ground vehicle (UGV), enhanced with lift capabilities, will possess greater ability to exert forces and torques on the environment. Despite the increasing complexity associated with the construction and control of these different types of vehicle, the advantages are numerous, with vast application areas (Omelchenko, 2004; Barnes et al., 2010).

This work proposes a novel unmanned vehicle that can operate as a UAV or UGV using a full 6-DOF tri-rotor platform for actuation. The full 6-DOF can be exploited whilst operating in the air, but will result in over-actuation whilst on the ground. When the UAV is embedded in an outer wheel structure, it can roll on the ground, thereby becoming a UGV. Since rolling is a more energy-efficient way of translating than flying, the vehicle flies only when it is necessary, perhaps due to autonomy tasks or as an obstruction avoidance strategy. The vehicle thus offers a platform to explore the problem of actuation and control from a tri-rotor's perspective vis-à-vis the problem of sta-

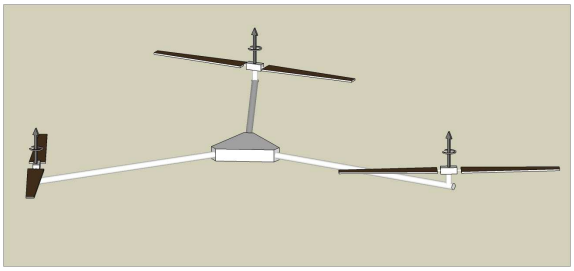

Figure 1: Tri-rotor UAV.

bilizing the wheeled-vehicle. The objective is to balance the vehicle in its unstable upright position, which invariably corresponds to solving the inverted pendulum problem in this highly coupled over-actuated system.

It is well-known that the robustness of control systems to disturbance and uncertainty is the central theme of feedback control (Zhou et al., 1996; Vinnicombe, 2001). Due to stringent performance and robust stability requirements and significant cross-coupling in the channels of the multi-input multi-output (MIMO) wheeled-vehicle, the $\mathscr{H}_\infty$ loop-shaping design procedure is used for the synthesis of a robust controller. This choice of controller synthesis is further justified since there is always a tradeoff between the accuracy and complexity of a model, bearing in mind that there are high fidelity dynamics that are neglected in the modelling, for example, higher order aerodynamics effects on the propellers.

$\mathscr{H}_\infty$ loop-shaping is a design paradigm that establishes a good tradeoff between performance and robustness of a closed-loop system by combining classical loop-shaping concepts with $\mathscr{H}_\infty$ synthesis. This, which can be easily adjusted in this design framework, is also intuitive for a control engineer. The controller maximizes the closed-loop robustness to coprime factor uncertainty, which has been shown to be a powerful type of unstructured uncertainty representation (Glover and McFarlane, 1989; Zhou et al., 1996; Lanzon and Papageorgiou, 2009). Since much of the design effort in $\mathscr{H}_\infty$ loop-shaping goes into the selection of the loop-shaping weights to achieve the desired performance specifications, the systematic framework established in (Osinuga et al., 2012a), which builds on (Osinuga et al., 2010; Osinuga et al., 2012b; Lanzon, 2005), is therefore used to simultaneously synthesize loop-shaping weights and a stabilizing controller that give satisfactory robust performance for a guaranteed level of robust stability margin.

The rest of the paper is organized as follows. The description of the vehicle is elucidated upon in Section 2 while the nonlinear model of the unmanned

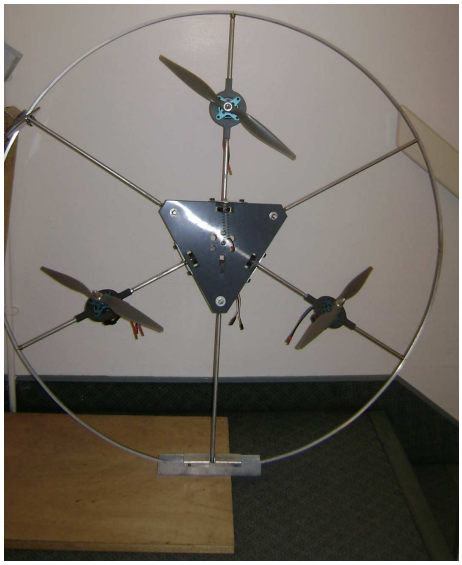

Figure 2: The proposed unmanned vehicle.

vehicle is derived in Section 3. In Section 4, input-output linearization technique is invoked to linearize the nonlinear dynamics around the upright operating point and a robust controller is subsequently synthesized. The concluding remarks and future scope of work are given in Section 5. Symbols and other notations are given in the appendix.

2 GENERAL DESCRIPTION OF THE UNMANNED VEHICLE

The proposed unmanned vehicle presented in this paper is shown in Figure 2 and its schematic diagram is shown in Figure 3(a), where

- there are six cylindrical spokes, connected to the centre of the circular wheel of a very small width of about 10mm; three of the spokes are used to support the propellers and their driving motors.
- (X_e, Y_e, Z_e) represents the earth coordinate system whereas (X_b, Y_b, Z_b) denotes the body coordinate system. $(X_{l_i}, Y_{l_i}, Z_{l_i})$ $\forall i = 1,2,3$ is the local coordinate system of the propeller-motor assembly, with the origin of each local coordinate system coinciding with the intersection of the UGV arm and the propeller-motor assembly, i.e., for $i = 1,2,3$, X_{l_i} is along the i^{th} arm of the UGV and Y_{l_i} is in the plane of the vehicle. When the servo angle is zero, the direction of the motor-shaft/propeller lift coincides with Z_{l_i};
- Figure 2 considers a reduced problem where the UGV is mechanically restricted to only rotate in

the roll direction ϕ_v around the X_e-axis while in contact with the ground. Denoting the angular velocity vector as $\omega^b = \begin{pmatrix} p & q & r \end{pmatrix}^T$, this restriction implies that $\theta_v = \psi_v = 0$ and $q = r = 0$.

The right hand coordinate system is used in this paper as shown in Figure 3(b).

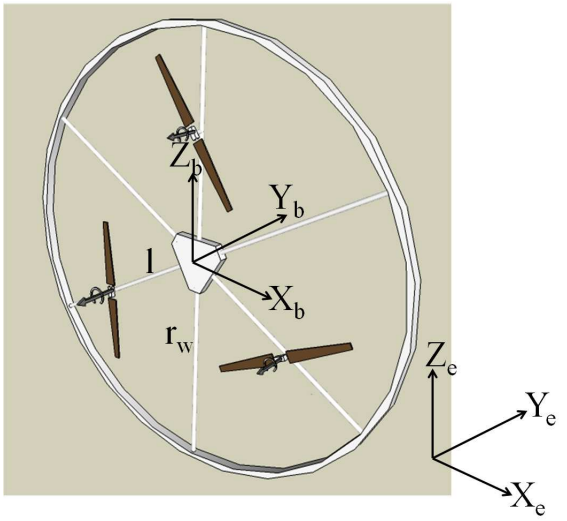

(a) Schematic diagram of the UGV.

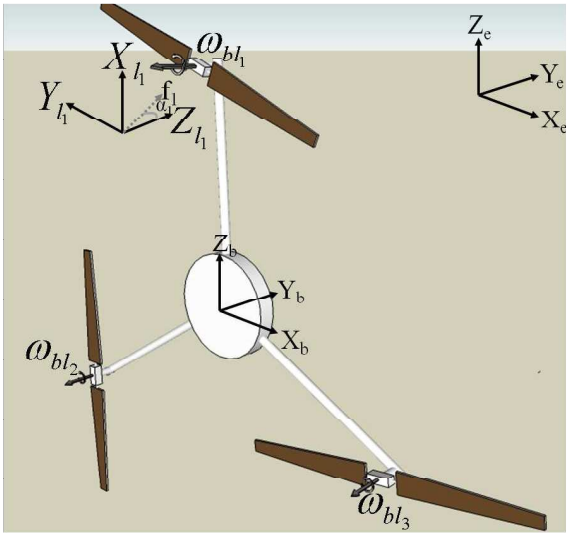

(b) Coordinate systems of the UGV.

Figure 3: Coordinate systems.

3 MATHEMATICAL MODEL OF THE UNMANNED VEHICLE

As earlier stated and also shown in Figure 2, the objective of this current work is to balance the UGV in its upright position ($\phi_v = 0$). Based on the local coordinate systems shown in Figure 3(a), the rotation angles from the propeller local coordinate system to the body coordinate system can be expressed as follows:

l_1 to b: $\phi^b_{l_1} = -90^\circ, \theta^b_{l_1} = 0^\circ, \psi^b_{l_1} = -90^\circ$;
l_2 to b: $\phi^b_{l_2} = -90^\circ, \theta^b_{l_2} = 0^\circ, \psi^b_{l_2} = 150^\circ$;
l_3 to b: $\phi^b_{l_3} = -90^\circ, \theta^b_{l_3} = 0^\circ, \psi^b_{l_3} = 30^\circ$.

The transformation from a fixed to a rotating coordinate system is obtained via a rotation matrix, and this is used to express the force and torque components in the local to the body coordinate system. The respective rotation matrices from the propeller local coordinate system to the body coordinate system are obtained as follows:

$$R^e_{l_1} = \begin{pmatrix} 0 & -1 & 0 \\ 0 & 0 & -1 \\ 1 & 0 & 0 \end{pmatrix}, R^e_{l_2} = \begin{pmatrix} -\frac{\sqrt{3}}{2} & \frac{1}{2} & 0 \\ 0 & 0 & -1 \\ -\frac{1}{2} & -\frac{\sqrt{3}}{2} & 0 \end{pmatrix}$$
$$R^e_{l_3} = \begin{pmatrix} \frac{\sqrt{3}}{2} & \frac{1}{2} & 0 \\ 0 & 0 & -1 \\ -\frac{1}{2} & \frac{\sqrt{3}}{2} & 0 \end{pmatrix}. \quad (1)$$

3.1 Actuator Dynamics

As part of the derivation of the model of the UGV, we start with the dynamics of the actuators. The dynamic equation of the BLDC[1] and the servo motors with their drive circuits can both be modelled as first order systems as follows:

$$\dot{\omega}_{bl} = \tau_{bl}\omega_{bl} + k_{bl}V_{bl}, \quad (2)$$
$$\dot{\alpha}_s = \tau_s\alpha_s + k_sV_s, \quad (3)$$

where $\omega_{bl} = \begin{bmatrix} \omega_{bl_1} \\ \omega_{bl_2} \\ \omega_{bl_3} \end{bmatrix}$, $\alpha_s = \begin{bmatrix} \alpha_{s_1} \\ \alpha_{s_2} \\ \alpha_{s_3} \end{bmatrix}$, $V_{bl} = \begin{bmatrix} V_{bl_1} \\ V_{bl_2} \\ V_{bl_3} \end{bmatrix}$ and $V_s = \begin{bmatrix} V_{s_1} \\ V_{s_2} \\ V_{s_3} \end{bmatrix}$, and ω_{bl_i} and α_{s_i} are expressed in the direction of rotation. In (2) and (3) above, it is assumed that the motors and servos have identical time constants, respectively. Note that τ_s (which is always negative) and k_s are directly obtained from the specifications of the servo drives while τ_{bl} and k_{bl} are calculated based on the specifications of the BLDC motors as follows:

$$\tau_{bl} = \frac{-k_v^2 + B_mR_a}{I_mR_a}; \; k_{bl} = \frac{k_v}{I_mR_a},$$

where $k_v^2 > B_mR_a$ (Ramu, 2009).

[1]Here, the inductance effect of the motors is neglected.

3.2 Forces

The total force acting on the UGV can be written as

$$F^b = F_p^b + F_g^b + F_r^b, \tag{4}$$

where F_p^b is the total propulsive force, F_g^b is the force due to gravity and F_r^b is the reaction force from the ground. Since the objective of the current work is to balance the UGV in its upright position, which is a precursor to rolling action, i.e., the vehicle is in contact with the ground, the force due to gravity is effectively cancelled by the reaction force in the earth coordinate system, even though there is torque attributed to these forces. The total propulsive force is equal to the algebraic sum of the individual propulsive forces generated by each propeller. The propulsive forces at the local coordinate systems can be written as

$$F_{p_i} = \begin{pmatrix} 0 \\ f_i \sin\alpha_{s_i} \\ f_i \cos\alpha_{s_i} \end{pmatrix} \forall i = 1,2,3. \tag{5}$$

The thrust generated by each propeller is ideally simplified as $f_i = k_f \omega_{bl_i}^2 \ \forall i = 1,2,3$. To obtain the propulsive forces in the body coordinate system, the rotation matrices obtained in (1) are used for the transformation to the body coordinate system:
$F_{p_i}^b = R_{l_i}^b F_{p_i} \ \forall i = 1,2,3$, thus yielding the following

$$F_{p_1}^b = \begin{pmatrix} F_{p_{1_x}}^b \\ F_{p_{1_y}}^b \\ F_{p_{1_z}}^b \end{pmatrix} = \begin{pmatrix} -k_f \omega_{bl_1}^2 \sin\alpha_{s_1} \\ -k_f \omega_{bl_1}^2 \cos\alpha_{s_1} \\ 0 \end{pmatrix}, \tag{6}$$

$$F_{p_2}^b = \begin{pmatrix} F_{p_{2_x}}^b \\ F_{p_{2_y}}^b \\ F_{p_{2_z}}^b \end{pmatrix} = \begin{pmatrix} \frac{1}{2} k_f \omega_{bl_2}^2 \sin\alpha_{s_2} \\ -k_f \omega_{bl_2}^2 \cos\alpha_{s_2} \\ -\frac{\sqrt{3}}{2} k_f \omega_{bl_2}^2 \sin\alpha_{s_2} \end{pmatrix}, \tag{7}$$

$$F_{p_3}^b = \begin{pmatrix} F_{p_{3_x}}^b \\ F_{p_{3_y}}^b \\ F_{p_{3_z}}^b \end{pmatrix} = \begin{pmatrix} \frac{1}{2} k_f \omega_{bl_3}^2 \sin\alpha_{s_3} \\ -k_f \omega_{bl_3}^2 \cos\alpha_{s_3} \\ \frac{\sqrt{3}}{2} k_f \omega_{bl_3}^2 \sin\alpha_{s_3} \end{pmatrix}. \tag{8}$$

Finally, the total propulsive force is obtained as

$$F_p^b = \sum_{i=1}^{3} F_{p_i}^b = k_f H_f \rho, \tag{9}$$

where $H_f = \begin{pmatrix} -1 & \frac{1}{2} & \frac{1}{2} & 0 & 0 & 0 \\ 0 & 0 & 0 & -1 & -1 & -1 \\ 0 & -\frac{\sqrt{3}}{2} & \frac{\sqrt{3}}{2} & 0 & 0 & 0 \end{pmatrix}$

and $\rho = \begin{pmatrix} \omega_{bl_1}^2 \sin\alpha_{s_1} \\ \omega_{bl_2}^2 \sin\alpha_{s_2} \\ \omega_{bl_3}^2 \sin\alpha_{s_3} \\ \omega_{bl_1}^2 \cos\alpha_{s_1} \\ \omega_{bl_2}^2 \cos\alpha_{s_2} \\ \omega_{bl_3}^2 \cos\alpha_{s_3} \end{pmatrix}$.

3.3 Torques

To simplify the complexity of the problem, we consider the different torques acting at the UGV's point of contact with the ground. Hence, the torque due to the reaction force F_r^b will be zero at this point. The total torque can now be written as

$$\tau^b = \tau_f^b + \tau_d^b + \tau_G^b + \tau_{gy}^b, \tag{10}$$

where τ_f^b is the torque due to the propulsive force, τ_d^b is the drag torque on the propellers, τ_G^b is the torque due to the force of gravity and τ_{gy}^b is the gyroscopic torque. The torque due to the thrust generated from the propellers with respect to the pivot point to the ground can be written as

$$\tau_f^b = k_f H_t \rho, \tag{11}$$

where

$$H_t = \begin{pmatrix} 0 & 0 & 0 & l + r_w & a & a \\ -l - r_w & b & b & 0 & 0 & 0 \\ 0 & 0 & 0 & 0 & \frac{\sqrt{3}}{2} l & -\frac{\sqrt{3}}{2} l \end{pmatrix},$$

where $a = r_w - \frac{l}{2}$ and $b = \frac{r_w}{2} - l$.

The drag torque, which is due to the rotation of the propeller, can be expressed in the local coordinate systems as

$$\tau_{d_{p_i}}^{l_1} = \begin{pmatrix} 0 \\ -k_t \omega_{bl_i}^2 \sin\alpha_{s_i} \\ -k_t \omega_{bl_i}^2 \cos\alpha_{s_i} \end{pmatrix} \forall i = 1,2,3.$$

The above torque is then expressed in the body coordinate system using the rotation matrices in (1) as $\tau_{d_{p_i}}^b = R_{l_i}^b \tau_{d_{p_i}}^{l_i} \ \forall i = 1,2,3$, and the resultant drag torque is obtained as

$$\tau_d^b = \sum_{i=1}^{3} \tau_{d_{p_i}}^b = -k_t H_f \rho. \tag{12}$$

The torque due to the force of gravity can be written as

$$\tau_G^b = M g r_w \begin{pmatrix} \sin\phi_v \\ 0 \\ 0 \end{pmatrix}. \tag{13}$$

Lastly, we derive the gyroscopic torque, which is as a result of the rotation of the UGV and the tilting of a rotating propeller. If we neglect the rotating parts of the BLDC motors, the gyroscopic torque can be modelled in the body coordinate as follows (Meriam and Kraige, 2010):

$$\begin{aligned} \tau_{gy_{p_i}}^b &= -I_p \left(\dot{\alpha}_{s_i}^b \times \omega_{bl_i}^b \right) - I_p \left(\omega^b \times \omega_{bl_i}^b \right), \\ &= -I_p \left(\dot{\alpha}_{s_i}^b + \omega^b \right) \times \omega_{bl_i}^b, \end{aligned} \tag{14}$$

where $\omega^b_{bl_i} := R^b_{l_i}\begin{bmatrix} 0 & \omega_{bl_i}\sin\alpha_{s_i} & \omega_{bl_i}\cos\alpha_{s_i}\end{bmatrix}^T$, $\dot{\alpha}^b_{s_i}$ is the rate of change in the tilting angle of the i^{th} servo motor, and is expressed as $\dot{\alpha}^b_{s_i} = R^b_{l_i}\begin{bmatrix} -\dot{\alpha}_{s_i} & 0 & 0\end{bmatrix}^T$.
Performing the algebraic manipulation in (14), the gyroscopic torques in the body coordinate system from the three propellers and the UGV are obtained as

$$\tau^b_{gy_{p_1}} = -I_p\omega_{bl_1}\begin{pmatrix} -\dot{\alpha}_{s_1}\cos\alpha_{s_1} \\ \dot{\alpha}_{s_1}\sin\alpha_{s_1} \\ -p\cos\alpha_{s_1}\end{pmatrix} \quad (15)$$

$$\tau^b_{gy_{p_2}} = -I_p\omega_{bl_2}\begin{pmatrix} \frac{1}{2}\dot{\alpha}_{s_2}\cos\alpha_{s_2} \\ (\dot{\alpha}_{s_2}+\frac{\sqrt{3}}{2}p)\sin\alpha_{s_2} \\ -(p+\frac{\sqrt{3}}{2}\dot{\alpha}_{s_2})\cos\alpha_{s_2}\end{pmatrix} \quad (16)$$

$$\tau^b_{gy_{p_3}} = -I_p\omega_{bl_3}\begin{pmatrix} \frac{1}{2}\dot{\alpha}_{s_3}\cos\alpha_{s_3} \\ (\dot{\alpha}_{s_3}-\frac{\sqrt{3}}{2}p)\sin\alpha_{s_3} \\ -(p-\frac{\sqrt{3}}{2}\dot{\alpha}_{s_3})\cos\alpha_{s_3}\end{pmatrix} \quad (17)$$

The total gyroscopic torque is given as the algebraic sum of (15) - (17): $\tau^b_{gy} = \sum_{i=1}^{3}\tau^b_{gy_{p_i}}$.

3.4 Dynamic Model

For the dynamic model of the vehicle, we use the Newton-Euler approach, and the translational and rotational dynamics can be written as follows:

$$F^e = \frac{\partial(M_{tot}\mathbf{v^e})}{\partial t} = M_{tot}\frac{\partial\mathbf{v^e}}{\partial t}, \quad (18)$$

$$\tau^e = \frac{\partial(I^e\omega^e)}{\partial t}. \quad (19)$$

Since all variables are expressed in the body coordinate system, the dynamic equations above can be equally rewritten in the body coordinate as follows:

$$F^b = M_{tot}\left(\dot{\mathbf{v}}^b + S\left(\omega^b\right)\mathbf{v}^b\right), \quad (20)$$

$$\tau^b = I^b\dot{\omega}^b + S\left(\omega^b\right)I^b\omega^b, \quad (21)$$

where $\mathbf{v}^b = \begin{pmatrix} u & v & w\end{pmatrix}^T$, $S\left(\omega^b\right)$ is the skew matrix of ω^b, given as

$$S\left(\omega^b\right) = \begin{pmatrix} 0 & 0 & 0 \\ 0 & 0 & -p \\ 0 & p & 0\end{pmatrix}, \text{ and}$$

$$I^b = \begin{pmatrix} I_{xx} & -I_{xy} & -I_{xz} \\ -I_{yx} & I_{yy} & -I_{yz} \\ -I_{zx} & -I_{zy} & I_{zz}\end{pmatrix}.$$

Due to the symmetry around the $y-z$ plane, $I_{yz} = I_{zy} = 0$. Also, note that $I_{xy} = I_{yx}$ and $I_{xz} = I_{zx}$.

Let the attitude and position vectors of the UGV in the earth coordinate system be denoted by $\eta := \begin{pmatrix}\phi_v & \theta_v & \psi_v\end{pmatrix}^T$ and $\lambda := \begin{pmatrix} x_v & y_v & z_v\end{pmatrix}^T$. Then, the following expressions, in addition to (20) and (21), fully describe the dynamic equations of the UGV:

$$\dot{\eta} = \Psi\omega^b \quad (22)$$

$$\dot{\lambda} = \left(R^b_e\right)^{-1}\mathbf{v}^b, \quad (23)$$

where R^b_e is the rotation matrix from the earth coordinate system to the body coordinate system and Ψ is the matrix that relates the angular velocity in the body coordinate system to the earth coordinate system (Valavanis, 2007; Freddi et al., 2011), both expressed as

$$R^b_e = \Psi = \begin{pmatrix} 1 & 0 & 0 \\ 0 & \cos\phi_v & -\sin\phi_v \\ 0 & \sin\phi_v & \cos\phi_v\end{pmatrix}. \quad (24)$$

Hence, the angular velocities are related in the body and the earth coordinate systems as $p = \dot{\phi}_v$.

Now, the dynamics governing the roll-axis rotation is obtained from the first row of (21):

$$\tau^b_x = I_{xx}\dot{p} = I_{xx}\ddot{\phi}_v, \quad (25)$$

where

$$\tau^b_x = k_f\left((l+r_w)\rho_4 + (r_w-\frac{l}{2})\rho_5 + (r_w-\frac{l}{2})\rho_6\right) - k_t\left(-\rho_1+\frac{1}{2}\rho_2+\frac{1}{2}\rho_3\right) + I_p\omega_{bl_1}\dot{\alpha}_{s_1}\cos\alpha_{s_1} - I_p\left(\frac{1}{2}\omega_{bl_2}\dot{\alpha}_{s_2}\cos\alpha_{s_2}+\frac{1}{2}\omega_{bl_3}\dot{\alpha}_{s_3}\cos\alpha_{s_3}\right) + Mgr_w\sin\phi_v. \quad (26)$$

4 DESIGN OBJECTIVES AND CONTROLLER SYNTHESIS

The control design objective of stabilizing the UGV in its unstable equilibrium point can be categorized under the generalized tracking and regulatory problems as follows: the controller should

1. ensure settling time of less than 2 secs;
2. ensure stability of the vehicle in an upright position ($\phi_v = 0$);
3. guarantee robustness of the system to input/output disturbance and measurement noise.

4.1 Input-output Linearization

In order to use the $\mathscr{H}_\infty$ loop-shaping design procedure to achieve the above objectives, we linearize the nonlinear dynamics of (26) using the Jacobi linearization and robust feedback linearization techniques. If we take ρ as the input to the vehicle, it is apparent that the gyroscopic torque is not affine in this input, but rather a nonlinear function of its components. We therefore do not consider this torque in the robust feedback linearization, but include it as a perturbation and uncertainty to the model. This is because the robust linearization technique of (Franco et al., 2006) requires affine control action. Also, the actuator dynamics are neglected in the controller design since they have much faster dynamics when compared with the dynamics of the UGV, and this is in line with the observation in (Aldhaheri and Khalil, 1996) that an output feedback controller recovers asymptotic stability in the presence of unmodelled fast actuator dynamics. Moreover, these dynamics are linear and there is therefore no need to cancel them. Albeit, both dynamics are fully incorporated in the time-domain simulations implemented in the next section.

Removing the gyroscopic term, we now take the input to the system in (25) as

$$\rho_\tau = k_f\left((l+r_w)\rho_4 + (r_w - \frac{l}{2})\rho_5 + (r_w - \frac{l}{2})\rho_6\right) - k_t\left(-\rho_1 + \frac{1}{2}\rho_2 + \frac{1}{2}\rho_3\right). \quad (27)$$

The resultant system can then be written as

$$\ddot{\phi}_v = \frac{1}{I_{xx}}(Mgr_w \sin\phi_v + \rho_\tau). \quad (28)$$

Now, invoking Jacobian linearization technique on the above state equation, the linearized model (about the equilibrium point $\phi_v = 0$, $\dot{\phi}_v = 0$, $\rho_\tau = 0$) can be written in state-space form as follows:

$$\begin{pmatrix} \dot{\phi}_v \\ \ddot{\phi}_v \end{pmatrix} = \begin{pmatrix} 0 & 1 \\ \frac{Mgr_w}{I_{xx}} & 0 \end{pmatrix}\begin{pmatrix} \phi_v \\ \dot{\phi}_v \end{pmatrix} + \begin{pmatrix} 0 \\ \frac{\rho_\tau}{I_{xx}} \end{pmatrix}, \quad (29)$$

and the output is ϕ_v.

Instead, one could also use the robust feedback linearization technique, proposed in (Franco et al., 2006), to linearize the nonlinear dynamics of the UGV. In order to get the parameters for this linearization technique, we first employ the classical feedback linearization method, choosing the output as $y = \phi_v$:

$$\dot{y} = y^{(1)} = \dot{\phi}_v; \quad (30)$$

$$\ddot{y} = y^{(2)} = \ddot{\phi}_v = \frac{1}{I_{xx}}(Mgr_w \sin\phi_v + \rho_\tau). \quad (31)$$

Let a new control input be defined as $\rho_\tau^c = \ddot{y}$, the classical feedback linearization law can then be written as:

$$\rho_\tau = I_{xx}\rho_\tau^c - Mgr_w \sin\phi_v. \quad (32)$$

From the above control law, the parameters for the robust feedback linearization can be written, using standard notation as in (Franco et al., 2006), as follows:

$$\alpha_c(\Phi) = -Mgr_w \sin\phi_v;$$
$$\beta_c(\Phi) = I_{xx};$$
$$\phi_c(\Phi) = \begin{pmatrix} \phi_v \\ \dot{\phi}_v \end{pmatrix},$$

where

$$\Phi = \begin{pmatrix} \phi_v & \dot{\phi}_v \end{pmatrix};$$
$$T = \left(\frac{\partial\phi_c(\Phi)}{\partial\Phi}\right)_{\Phi=0} = \begin{pmatrix} 1 & 0 \\ 0 & 1 \end{pmatrix};$$
$$R = \beta_c(0) = I_{xx};$$
$$L = -R^{-1}\left(\frac{\partial\alpha_c(\Phi)}{\partial\Phi}\right)_{\Phi=0} = \begin{bmatrix} I_{xx}^{-1}Mgr_w & 0 \end{bmatrix}.$$

Now, the new control law is given as

$$\rho_\tau = \alpha + \beta\rho_\tau^r, \quad (33)$$

where ρ_τ^r is the linear control effort and

$$\alpha = \alpha_c(\Phi) + \beta_c LT^{-1}\phi_c(\Phi) = Mgr_w(\phi_v - \sin\phi_v);$$
$$\beta = \beta_c R^{-1} = 1,$$

with the linearized model given in state-space form as in (29), with ρ_τ replaced with ρ_τ^r.

Remark 1. *(a) The choice of ρ_τ as input to the system is quite intuitive as it is derived from the force/torque mapping to the input to the plant. The forces in x, y and z directions and torques in y and z directions can be set to zero so that there will be no exerted forces and torques in undesirable directions.*

(b) The solution to the stabilization problem depends on the non-singularity of the mapping from $\begin{pmatrix} F_p^b \\ \tau_f^b + \tau_d^b \end{pmatrix}$ to ρ. This mapping is intrinsic to the mechanical structure of the vehicle, i.e., the position and orientation of the propeller-motor assembly, the orientation of the servo motors, etc. The proposed mechanical structure of the vehicle is therefore sensible since this term always has full rank and is not ill-conditioned. This signifies that there always exists a combination of inputs for any choice of force and torque. Note that the output of the controller is ρ_x^b and the force/torque mapping is used to obtain the required ρ.

4.2 Robust Controller Synthesis

As earlier motivated, the $\mathscr{H}_\infty$ loop-shaping design procedure is used for the controller synthesis and the following considerations (in view of the design specifications stated at the beginning of this section 5) are made in the selection of weights to form the shaped plant P_s, which is the cascade between the loop-shaping weights W_1 and W_2 and the nominal plant:

- for good reference signal tracking and input disturbance rejection in (a) and (c), respectively, a designer maximizes the loop-gain of the shaped plant P_s at low frequencies in order to obtain a small sensitivity function;
- for fast response in (a), a reasonable bandwidth is required;
- for good robustness to unmodelled dynamics and sensor noise in (c), the designer's objective is to minimize the loop-gain of the shaped plant P_s in order to make the complementary sensitivity transfer function matrix close to zero;
- for robust stability of the UGV in (b), the objective is to maximize the gain and phase margins so as to avoid a perturbed plant encircling the Nyquist point. In (Glover et al., 2000; Vinnicombe, 2001), the relationships between the robust stability margin $b(P_s,C_\infty)$ and the gain and phase margins have been established; $b(P_s,C_\infty)$ of 0.3 is equivalent to a gain and phase margins greater than or equal to 5.39dB and 34.92°, respectively.

An algorithm in (Osinuga et al., 2011; Osinuga et al., 2012a) directly captures the above factors in a systematic manner, and will therefore be used to synthesize a controller for the linearized plants. This efficient framework simultaneously synthesizes loop-shaping weights and a stabilizing controller that achieve satisfactory performance for a guaranteed level of robust stability margin, corresponding to sufficient gain and phase margins of the closed-loop system. This algorithm also incorporates smoothness constraints, formulated in (Osinuga et al., 2010), to aid the synthesis of low-order, "smooth" controller that avoids the "approximate" pole-zero cancellation of the lightly-damped modes of the nominal plant.

The inputs to this algorithm are simply chosen as: $[\overline{w}_1\ \underline{w}_1\ k_1\ g_1\ \omega_l\ \omega_u\ \overline{\varepsilon}] = [10^{-2}\ 10^2\ 1\ 60\ 0.1\ 80\ 0.3]$, where $\overline{w}_1(\mathtt{rad/s})$, $\underline{w}_1(\mathtt{rad/s})$, k_1 and $g_1(\mathtt{dB/dec})$ respectively delimit the allowable region for the singular values, condition number and gradient of loop-shaping weight W_1, $\omega_l(\mathtt{rad/s})$ and $\omega_u(\mathtt{rad/s})$ divide the frequency region into three distinct frequency regions of low, mid and high frequencies, respectively, while $\overline{\varepsilon}$ is the desired level of robust stability margin that is chosen 'a priori'. Here, frequency points between 10^{-3} and 10^3 `rad/s` are divided into 150 equally spaced points on a logarithmical scale. Furthermore, we fix the post-compensator as a first-order low-pass filter with a corner frequency of `50rad/s`.

The algorithm converged in four iterations, and the order of the synthesized pre-compensator is 8. A robust stability margin of 0.4608 is obtained, which is an indicator of a decent design that tolerates approximately 46% coprime factor uncertainty for which closed-loop stability is guaranteed. The singular values of the nominal plant P, the correspondingly shaped plant P_s, the simultaneously synthesized stabilizing controller and synthesized loop-shaping weight are shown in Figure 4.

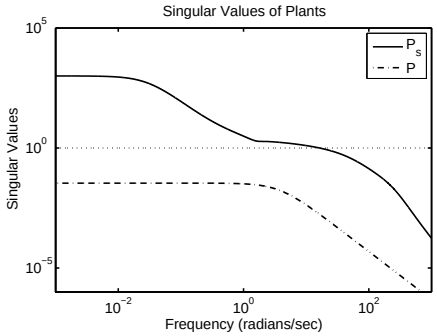

(a) Singular values of the linearized nominal and shaped plant.

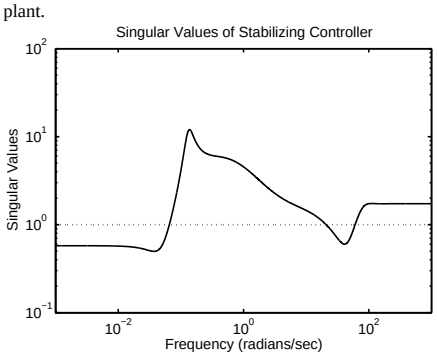

(b) Singular values of the robust stabilizing controller.

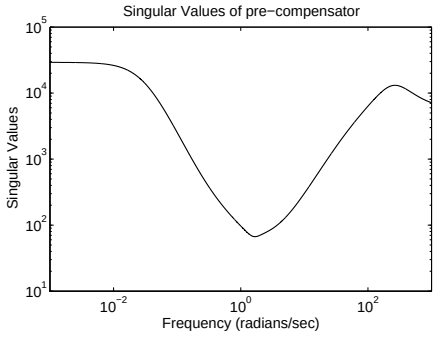

(c) Singular values of the synthesized pre-compensator.

Figure 4.

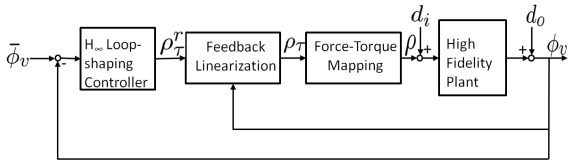

Figure 5: Simulation block diagram: High Fidelity Plant includes gyroscopic dynamics, ignored in the control systems design.

5 SIMULATION RESULTS

We set up the simulation in Simulink[2] as shown in Figure 5. A non-zero initial state of the inverted pendulum-based vehicle was set as $\phi_v = 0.18\mathtt{rad}$ and the desired reference input signal was given as $\phi_v = 0$. For the simulation, the roll channel was perturbed with an output disturbance of maximum magnitude of $0.13\mathtt{rad}$ from time $t = 10s$ to $t = 12s$; BLDC and servo output disturbance of $10.5\mathtt{rad/s}$ and $0.09\mathtt{rad}$ (corrupted with uniform random noise) were further introduced from $t = 15s$ to $t = 17s$.

For both simulations involving the Jacobian and the robust feedback linearization techniques, the plots of the angular acceleration, angular velocity and the orientation of the CG of the UGV, alongside the gyroscopic torque are shown in Figure 6, where it is seen that all the states are well-behaved.

It is evident that the two control schemes stabilized the vehicle in its upright position. The speed of the responses were very fast, satisfying the desired specification. Also, the robust controller adequately recovered from the effect of input and output disturbance, and the overall response and damping was satisfactory. Furthermore, the BLDC and servo motors were bounded within the limits of 900 $\mathtt{rad/s}$ and $\pm\pi\mathtt{rad}$, respectively, as shown in Figure 7. Finally, the gyroscopic torque, considered as unaccounted perturbation to the system, was well-handled by the controller.

Remark 2. *(a) As expected, the closed-loop system with the robust feedback linearization technique showed slightly better performance; the output mean square error values of 16.9761 and 18.0834 were, respectively, obtained from the robust feedback linearization and Jacobi linearization techniques. It should be noted that the robust feedback linearization produces a linear system that coincides with the Jacobi linearized system. However, the robust feedback linearization is effectively a robust nonlinear controller that uses the concept of 'local W-stability' to guarantee the local input-output stability of the nonlinear system, thereby preserving the robustness properties of the linear design (Franco et al., 2006). Hence, whereas a Jacobi linearization is just an approx-*

[2]The feedback linearization block is removed when implementing the Jacobian linearization technique.

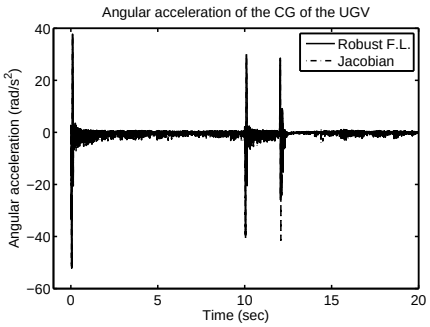

(a) Angular acceleration of the pivot point of the UGV.

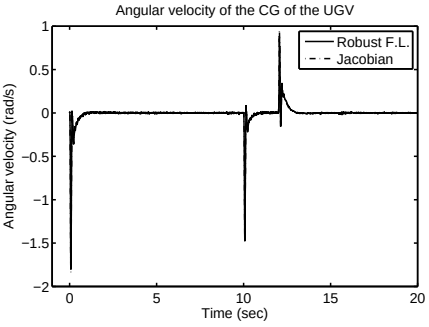

(b) Angular velocity of the pivot point of the UGV.

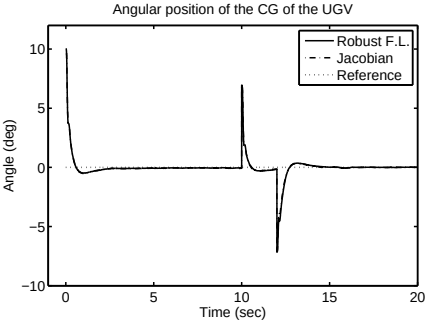

(c) Angular position of the pivot point of the UGV.

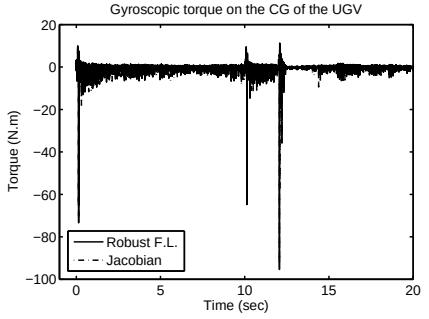

(d) Gyroscopic torque.

Figure 6: Angular acceleration, velocity and position of the vehicle and gyroscopic torque.

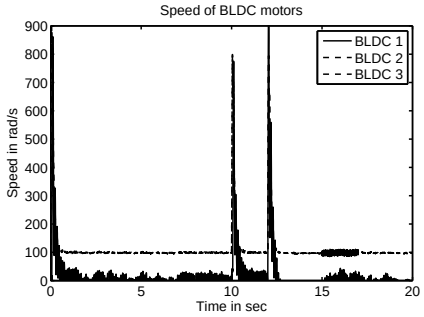

(a) Speed of the BLDC motors.

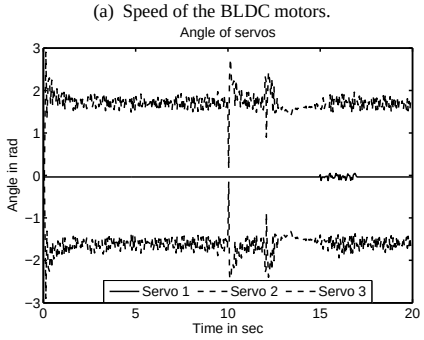

(b) Angles of the servo motors.

Figure 7: Actuator efforts.

imation at an operating point, a robust feedback linearization is an exact nonlinear linearization of the same model.

(b) The force along the Z_e-axis was chosen as 5N*, which is about* 10% *of the UGV's weight. A non-zero positive force in this axis was chosen in order to operate the motors adequately in optimal region.*

6 CONCLUSIONS

A novel 6-DOF, tri-rotor actuated vehicle is presented in this paper. The nonlinear dynamics of the unmanned vehicle are developed and linearized using the Jacobi linearization and the robust feedback linearization techniques. A robust stabilizing controller is thereafter synthesized using a systematic weight optimization algorithm in $\mathscr{H}_\infty$ loop-shaping control and this choice of controller synthesis technique is demonstrated to be robust and effective; the time-domain simulations showed satisfactory tracking performance and disturbance rejection characteristics. Future work will involve experimental validation and controller tuning.

REFERENCES

Aldhaheri, R. and Khalil, H. (1996). Effect of unmodeled actuator dynamics on output feedback stabilization of nonlinear systems. *Automatica*, 32(9):1323–1327.

Barnes, L., Garcia, R., Fields, M., and Valavanis, K. (2010). Adaptive swarm formation control for hybrid ground and aerial assets. *Cutting Edge Robotics*, pages 263–278.

Crowther, B., Lanzon, A., Maya-Gonzalez, M., and Langkamp, D. (2011). Kinematic analysis and control design for a non planar multirotor vehicle. *AIAA Journal of Guidance, Control and Dynamics*, 34(4):1157–1171.

Crowther, W., Lanzon, A., Pilmoor, M., and Geoghegan, P. (2010). Rotary wing vehicle. *U.K. Patent GB2462452A*.

Das, A., Subbarao, K., and Lewis, F. (2009). Dynamic inversion with zero-dynamics stabilisation for quadrotor control. *IET Control Theory and Applications*, 3(3):303–314.

Escareño, J., Sanchez, A., and Lozano, G. (2008). Triple tilting rotor mini-uav: Modeling and embedded control of the attitude. *Proceedings of the American Control Conference, Seattle, Washington*, pages 3476–3481.

Franco, A., Bourles, H., De Pieri, E., and Guillard, H. (2006). Robust nonlinear control associating robust feedback linearization and $\mathscr{H}_\infty$ control. *IEEE Transactions on Automatic Control*, 51(7):1200–1207.

Freddi, A., Lanzon, A., and Longhi, S. (2011). A feedback linearization approach to fault tolerance in quadrotor vehicles. *Proceedings of the 18th IFAC World Congress, Milan, Italy*, pages 5413 – 5418.

Glover, K. and McFarlane, D. (1989). Robust stabilization of normalized coprime factor plant descriptions with $\mathscr{H}_\infty$-bounded uncertainty. *IEEE Transactions on Automatic Control*, 34(8):821–830.

Glover, K., Vinnicombe, G., and Papageorgiou, G. (2000). Guaranteed multi-loop stability margins and the gap metric. *Proceedings of IEEE Conference on Decision and Control, Sydney, Australia*, pages 4084–4085.

Kim, H. and Shim, D. (2003). A flight control system for aerial robots: algorithms and experiments. *Control Engineering Practice*, 11:1389–1400.

Lanzon, A. (2005). Weight optimisation in $\mathscr{H}_\infty$ loop-shaping. *Automatica*, 41(1):1201–1208.

Lanzon, A. and Papageorgiou, G. (2009). Distance measures for uncertain linear systems: A general theory. *IEEE Transactions on Automatic Control*, 54(7):1532–1547.

Lum, C. and Waggoner, B. (2011). A risk based paradigm and model for unmanned aerial systems in the national airspace. *Proceedings of the AIAA Infotech@Aerospace Conference, Missouri*.

Meriam, J. and Kraige, L. (2010). *Engineering mechanics: Dynamics*, volume 2. John Wiley and Sons.

Omelchenko, A. (2004). Avionics systems design for cooperative unmanned air and ground vehicles. *Ph.D. thesis, Department of Aeronautics and Astronautics, Massachusetts Institute of Technology*.

Osinuga, M., Patra, S., and Lanzon, A. (2010). Smooth weight optimization in $\mathscr{H}_\infty$ loop-shaping design. *Systems and Control Letters*, 59:663–670.

Osinuga, M., Patra, S., and Lanzon, A. (2011). Weight optimization for maximizing robust performance in $\mathscr{H}_\infty$ loop-shaping design. *Proceedings of the 18th IFAC World Congress, Milan, Italy*, pages 10135 – 10140.

Osinuga, M., Patra, S., and Lanzon, A. (2012a). An iterative algorithm for maximizing robust performance in $\mathscr{H}_\infty$ loop-shaping design. *International Journal of Robust and Nonlinear Control, In Press*.

Osinuga, M., Patra, S., and Lanzon, A. (2012b). State-space solution to weight optimization problem in $\mathscr{H}_\infty$ loop-shaping control. *Automatica*, 48(3):505–513.

Prior, S., Shen, S., White, A., Odedra, S., Karamanoglu, M., Erbil, M., and Foran, T. (2009). Development of a novel platform for greater situational awareness in the urban military terrain. *Lecture Notes in Computer Science: Engineering Psychology and Cognitive Ergonomics. Springer Berlin*, 5639:120–125.

Ramu, K. (2009). *Permanent magnet synchronous and brushless DC motors.* Marcel Dekker Inc.

Salazar-Cruz, S., Kendoul, F., Lozano, R., and Fantoni, I. (2006). Real-time control of a small-scale helicopter having three rotors. *Proceedings of the International Conference on Intelligent Robots and Systems, Beijing*, pages 2924–2929.

Valavanis, K. (2007). *Advances in Unmanned Aerial Vehicles: State of the Art and the Road to Autonomy*, volume 33. Intelligent Systems, Control and Automation: Science and Engineering, Springer.

Vinnicombe, G. (2001). *Uncertainty and feedback: $\mathscr{H}_\infty$ loop-shaping and v-gap metric.* Imperial College Press.

Yoo, D., Oh, H., Won, D., and Tahk, M. (2010). Dynamic modeling and stabilization techniques for tri-rotor unmanned aerial vehicles. *International Journal of Aeronautical and Space Science*, 11(3):167–174.

Zhou, K., Doyle, J., and Glover, K. (1996). *Robust and optimal control*. Englewood Cliffs, NJ: Prentice Hall.

APPENDIX

Let the feedback interconnection of a shaped plant $P_s = W_2 P W_1$ and a robust stabilizing controller C_∞ be denoted by $[P_s, C_\infty]$. Furthermore, let $\mathscr{C}(P_s)$ denote the set of all stabilizing controllers for P_s (i.e., $\mathscr{C}(P_s) := \{C_\infty : [P_s, C_\infty] \text{ is internally stable}\}$), the robust stability margin of $[P_s, C_\infty]$ is then defined as

$$b(P_s, C_\infty) := \left\| \begin{bmatrix} P_s \\ I \end{bmatrix} (I - C_\infty P_s)^{-1} \begin{bmatrix} -C_\infty & I \end{bmatrix} \right\|_\infty^{-1}$$

when $C_\infty \in \mathscr{C}(P_s)$, and 0 otherwise.

Symbol	Description
V_{bl_i}	Applied voltage to the i^{th} Brushless DC (BLDC) motor
V_{s_i}	Applied voltage to the i^{th} servo motor
τ_{bl}	Time constant of BLDC motor (0.035s)
k_{bl}	Gain of BLDC motor (10.81)
k_s	Gain of servo motor (0.02)
τ_s	Time constant of servo motor (0.018s)
ω_{bl_i}	Rotational speed of the i^{th} BLDC motor
α_{s_i}	Tilting angle of the i^{th} servo motor
f_i	Generated propulsive force in the direction of the motor shaft
k_f	Thrust constant of propeller
k_t	Torque constant of drag resulting from the rotation of propeller
g	Gravitational acceleration
M	Total mass of the unmanned vehicle
l	Distance between propeller-motor assembly and the centre of gravity of the unmanned vehicle
r_w	Radius of the vehicle's wheel
I_p	Inertia of propeller around axis of rotation
I_m	Inertia of rotor of BLDC motor
R_a	Armature resistance of BLDC motor
B_m	Viscous friction coefficient of propeller
k_v	Speed-to-voltage constant of BLDC motor
$\mathbf{v}$	Velocity vector of the unmanned vehicle
ω	Angular velocity vector of the unmanned vehicle
$(\phi_v, \theta_v, \psi_v)$	Roll, pitch and yaw angles of the unmanned vehicle
(x_v, y_v, z_v)	x, y, z position of the unmanned vehicle
$\mathbf{a}^b$, $\mathbf{a}^e$	vector $\mathbf{a}$ in the body and earth coordinate system, respectively